ISSN 1995-0802, Lobachevskii Journal of Mathematics, 2017, Vol. 38, No. 5, pp. 978–985. © Pleiades Publishing, Ltd., 2017.

Generalized Ensemble Computer Simulations for Structure Formation of Semiflexible Polymers

W. Janke[1*], M. Marenz[1], and J. Zierenberg[1]

(Submitted by L. N. Shchur)

[1] *Institut für Theoretische Physik, Universität Leipzig, Postfach 100 920, D-04009 Leipzig, Germany*

Received September 27, 2016

Abstract—Over the last two decades generalized ensemble Monte Carlo computer simulation studies employing multicanonical, Wang–Landau, or replica-exchange methods have proven to be a strong numerical tool for investigations of the statistical physics of polymer chains.
After a discussion of the theoretical background of these approaches, their power will be demonstrated in two applications to coarse-grained models of semiflexible polymers, which show a rich variety of structural motifs such as hairpins, knots and twisted bundles.

DOI: 10.1134/S1995080217050171

Keywords and phrases: *Monte Carlo simulations, multicanonical method, semiflexible polymers*.

1. INTRODUCTION

Monte Carlo computer simulations of the statistical physics of polymer systems is a very rich field with countless practical applications ranging from nanotechnology over molecular biology to all kinds of plastics. By stochastically sampling the state space with a Markov chain, the simulations provide thermodynamic and structural information of the system. The latter is particularly important for polymers whose typically line-like structure gives rise to many different structural motifs. Depending on the application at hand and on how chemically realistic the employed models are, the simulation outcome may be compared either directly with experimental data or with analytical predictions.

Computer simulations have thus become the third cornerstone of modern polymer science beyond experiments and analytical theory. The great success of computer simulations derives in part from the continuously improving hardware, but even more from methodological improvements of the software.

Among them, prominent approaches are multicanonical and parallel tempering Monte Carlo simulation methods as well as microcanonical analysis tools which will be described in Sec. 2. The usefulness of these approaches will be demonstrated in Sec. 3 for two physically relevant applications in polymer research: The bulk phase diagram of a semiflexible polymer covering the full range from flexible to stiff and the aggregation process of a few semiflexible polymers in dilute solution. In this short overview we mainly focus on our own research projects. More comprehensive recent reviews of the state-of-the-art in this field and complementary references to related work are given in [1, 2]. The paper concludes with a summary in Sec. 4.

2. COMPUTATIONAL METHODS

In this section we first focus on combinations of multicanonical [3–6] and replica-exchange [7] methods: Generalized ensemble methods we actually employed in the applications discussed in Sec. 3. For a comprehensive comparison with the Wang–Landau approach [8, 9], see [1]. We conclude this section with a brief sketch of the microcanonical analysis framework.

*E-mail: wolfhard.janke@itp.uni-leipzig.de

2.1. Multicanonical (Muca) Simulations

The multicanonical method [3–6] is basically a two-step process, where one first determines iteratively an a priori unknown weight function $W(E)$ for microstates x (e.g., polymer configurations) with system energy $E(x)$ which replaces the Boltzmann weight $\mathrm{e}^{-\beta E}$ in the canonical partition function

$$Z(T) = \sum_x \mathrm{e}^{-\beta E(x)} = \sum_E g(E)\mathrm{e}^{-\beta E} \to Z_{\mathrm{muca}} = \sum_x W\left(E\left(x\right)\right) = \sum_E g(E)W(E), \tag{1}$$

where $\beta = 1/k_B T$ is the inverse temperature and $g(E)$ the density of states (in the following we use natural units where $k_B = 1$). In most applications one aims at adjusting the multicanonical weight $W(E)$ such that the transition probabilities between microstates with different energies become roughly constant,

$$H(E) \propto P_{\mathrm{muca}}(E) = g(E)W(E) \approx \mathrm{const}, \tag{2}$$

giving an approximately flat energy histogram and hence a random-walk like time evolution of the Markov chain. The canonical acceptance probability of Monte Carlo update moves $x \to x'$ has then to be modified to

$$p_{\mathrm{acc}}(x \to x') = \min\left\{1, \mathrm{e}^{-\beta(E(x')-E(x))}\right\} \to \min\left\{1, \frac{W(E(x'))}{W(E(x))}\right\}.$$

The solution of (2) is $W(E) \propto g^{-1}(E)$. The density of states $g(E)$, however, is usually not known beforehand (otherwise a simulation would hardly be necessary). Instead one has to seek a solution by iteration. This can be initialized with $W(E) = W^{(0)}(E) \equiv 1$ in (1), corresponding to a standard canonical simulation at $\beta = 0$. The resulting energy histogram $H^{(0)}(E)$ ($\propto P_{\beta=0}(E)$) is then used to compute an improved weight estimate $W^{(1)}(E) = W^{(0)}(E)/H^{(0)}(E)$. The following run with $W^{(1)}(E)$ in (1) gives $H^{(1)}(E)$, resulting in the next estimate $W^{(2)}(E) = W^{(1)}(E)/H^{(1)}(E)$, and in general

$$W^{(n+1)}(E) = W^{(n)}(E)/H^{(n)}(E). \tag{3}$$

Once the energy histogram satisfies $H^{(n)}(E) \approx \mathrm{const}$, i.e., is sufficiently flat, $W^{(n+1)}(E) \simeq W^{(n)}(E) \simeq g^{-1}(E)$ is at a fixed point of the iteration and, up to statistical fluctuations, will no longer vary systematically.

This iteration can easily be parallelized [10, 11]. Instead of simulating the system only once, one considers m independent copies that have identical weights $W^{(n)}(E)$ but start with a different seed for the random number generator and thus realize different Markov chains. After each iteration the histograms $H_i^{(n)}(E)$ of all replicas are summed up to give $H^{(n)}(E) = \sum_{i=1}^m H_i^{(n)}(E)$, which is then used in (3) to obtain the next weight $W^{(n+1)}(E)$. This enables one to use many CPU cores in parallel or even the massively parallel architecture of GPUs [12], which drastically reduces the needed wall-clock time for a multicanonical simulation.

Once the multicanonical weight $W(E)$ is determined, it is kept fixed. After a thermalization period, a long production run is performed to compute for any quantity O the canonical expectation value by inverse reweighting,

$$\langle O\rangle(\beta) = \langle O\mathrm{e}^{-\beta E}W(E)^{-1}\rangle_{\mathrm{muca}}/\langle \mathrm{e}^{-\beta E}W(E)^{-1}\rangle_{\mathrm{muca}}.$$

This can be estimated as usual by the mean value over a time series with N measurements, $\overline{O}(\beta) = \sum_{i=1}^N O_i \mathrm{e}^{-\beta E_i}W(E_i)^{-1}/\sum_{i=1}^N \mathrm{e}^{-\beta E_i}W(E_i)^{-1}$.

2.2. Replica-Exchange (RE) Simulations

The replica-exchange approach [7] (also often referred to as parallel tempering) follows a different strategy and simulates m replicas at different temperatures $T_\mu = 1/\beta_\mu$. Every now and then the microstates x_μ and x_ν of two (usually neighboring) replicas μ and ν are proposed to be exchanged. Detailed balance is ensured if such exchanges are accepted with probability

$$p_{\mathrm{acc}}\left(x_\mu \leftrightarrow x_\nu\right) = \min\left\{1, \exp\left(\Delta\beta\Delta E\right)\right\}, \tag{4}$$

where we used the abbreviations $E_\mu = E(x_\mu)$, $E_\nu = E(x_\nu)$, and $\Delta X = X_\mu - X_\nu$. For additive energies of the form $E = E_1 + \kappa E_2$ this can easily be generalized to a two-dimensional RE variant (2DRE), where m different parameter pairs $(\beta, \kappa)_\mu$ are simulated at once. Here, the probability for an exchange $x_\mu \leftrightarrow x_\nu$ is given by (4) with $\Delta\beta\Delta E \to \Delta\beta\Delta E_1 + \Delta(\beta\kappa)\Delta E_2$. In the two-dimensional parameter space, it is easier to circumvent topological barriers which otherwise could hinder the one-dimensional flux of the replicas.

2.3. Multicanonical Replica-Exchange (Muca + RE) Simulations

Also multicanonical simulations can still get stuck when there are barriers in phase space that are not reflected in the energy distribution $p(E)$, but rather in observables "orthogonal" to E.

To cope with this problem, one may combine the multicanonical method in the energy direction with replica exchange in an "orthogonal" direction [13]. For an energy of the form $E = E_1 + \kappa E_2$, one may simulate m replicas at different parameters κ_μ along the "orthogonal" direction. The only difference is that in this case the underlying method is a multicanonical simulation at κ_μ using a weight $W_\mu(E)$ instead of the canonical Boltzmann factor. The replica-exchange probability (4) hence generalizes to ($E_{1,\mu} = E_1(x_\mu)$ etc.)

$$p_{\mathrm{acc}}\left(x_\mu \leftrightarrow x_\nu\right) = \min\left\{1, \frac{W_\mu(E_{1,\nu} + \kappa_\mu E_{2,\nu}) W_\nu(E_{1,\mu} + \kappa_\nu E_{2,\mu})}{W_\mu(E_{1,\mu} + \kappa_\mu E_{2,\mu}) W_\nu(E_{1,\nu} + \kappa_\nu E_{2,\nu})}\right\}.$$

2.4. Microcanonical Analysis

Generalized ensemble methods give direct access to the density of states $g(E)$, up to an overall normalization constant. They are thus perfectly suited for a microcanonical analysis [14–17], where one defines the conformational entropy $S(E) = \ln g(E)$ and its successive derivatives, the conformational microcanonical inverse temperature $\beta(E) = dS(E)/dE = d\ln g(E)/dE$ and $\gamma(E) = d\beta(E)/dE$. This encodes all relevant transitions for which the energy is a suitable reaction coordinate and allows for a classification of the transition order for finite systems [14–17]. If $\beta(E)$ shows a back-bending, which corresponds to a positive peak in $\gamma(E)$, the transition may be classified first order. This is equivalent to a double-peak energy probability distribution in the canonical ensemble [15]. If $\beta(E)$ shows an inflection point with negative slope, i.e., a negative peak in $\gamma(E)$, the transition is of second order instead. Such an analysis has turned out to be very helpful, especially when signals of several transitions overlap in the canonical ensemble.

Note that in most Monte Carlo studies, E has the meaning of the potential energy (because the momenta contributing to the kinetic energy can be integrated out exactly). The considered microcanonical quantities are hence strictly speaking not identical to the ones discussed in most textbooks on statistical mechanics where usually the total energy (sum of kinetic and potential energy) is considered. For a recent discussion of the mapping to the full microcanonical ensemble in terms of the total energy in a Monte Carlo simulation, see [18, 19].

3. APPLICATIONS

In this section we discuss two polymer applications which illustrate what can be achieved with the quite sophisticated simulation and analysis techniques outlined above.

3.1. Bulk Phase Diagram of Semiflexible Polymers

We consider a minimalistic coarse-grained bead-stick model of a linear polymer with fixed bond length (normalized to unity) where two terms contribute to the energy:

$$E = 4\epsilon \sum_{i=1}^{N-2} \sum_{j=i+2}^{N} \left[\left(\frac{\sigma}{r_{ij}}\right)^{12} - \left(\frac{\sigma}{r_{ij}}\right)^{6}\right] + \kappa \sum_{i=1}^{N-2} \left(1 - \cos\vartheta_i\right). \tag{5}$$

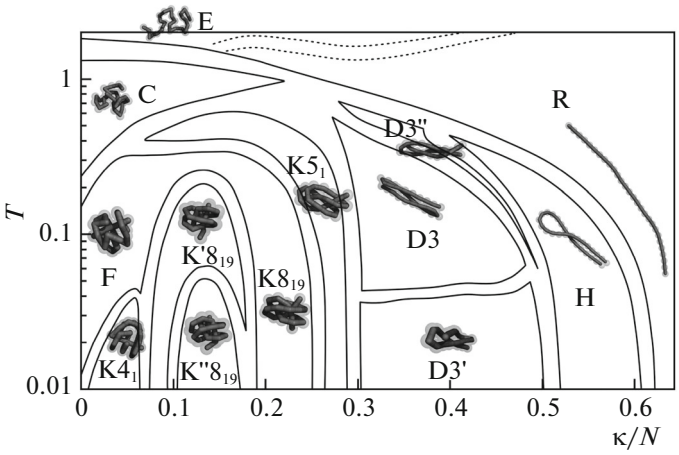

Fig. 1. Bulk phase diagram of a semiflexible 28mer in the temperature—bending stiffness plane (E: elongated, R: rod-like, C: collapsed, F: frozen, K: knotted, DN: N aligned strands, H: hairpin).

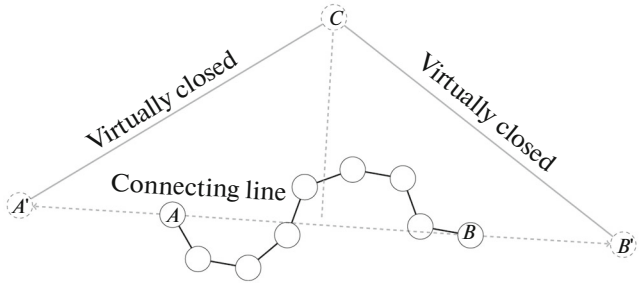

Fig. 2. Sketch of the employed prescription to close an open polymer virtually.

The first term is a standard 12-6 Lennard–Jones (LJ) potential, where r_{ij} measures the distance between monomers i and j. The parameters ϵ and σ set the energy and length scales, respectively, taken to be unity in the following. The second term models the bending energy, where $0 \leq \vartheta_i \leq \pi$ is the bending angle between adjacent bonds and κ is the stiffness parameter.

Figure 1 shows the pseudophase diagram for a 28mer obtained with 2DRE and muca+RE simulations [20–22]. The most intriguing observation is that the diagram exhibits stable phases that are characterized by knotted polymer chains (denoted by K). The other structural motifs (R: rod-like, C: collapsed, F: frozen, DN: bended with N aligned strands, H: hairpin) are similar to those observed in a quite similar bead-*spring* model [23, 24], where the knot phases, however, do not occur.

Closer inspection of the knotted chains reveals that they are mainly of type $C_n = 5_1$ and 8_{19} according to the usual classification scheme, showing that the chains preferentially form so-called torus knots. The integer C counts the minimal number of crossings of any projection of a knot onto a two-dimensional plane and the subscript n distinguishes topologically different knots with the same C. For the identification of the knot type we employed a method described in [25], where a specific product $\Delta_p(t) \equiv |\Delta(t) \times \Delta(1/t)|$ of the Alexander polynomial $\Delta(t)$ is evaluated at $t = -1.1$. For definitions and a detailed exposition of mathematical knot theory, see [26].

The identification of knots in an open polymer requires some prescription of how to close its two ends virtually. If one would just connect the two termini by a straight line, this would result in quite complicated knots when the polymer is very compact. This clearly must be considered as an artefact. We therefore employed the more sophisticated closure sketched in Fig. 2, which is inspired by tying a real knot. First one connects the termini by a straight line, which is then extended in both directions to the virtual end points A' and B' far away from all monomers. The polymer is then closed via straight lines connecting A' and B' with a far away point C on the perpendicular bisector of the connecting line. We checked that this procedure is numerically stable, i.e., any reasonably defined closure results with high probability in the same knot type.

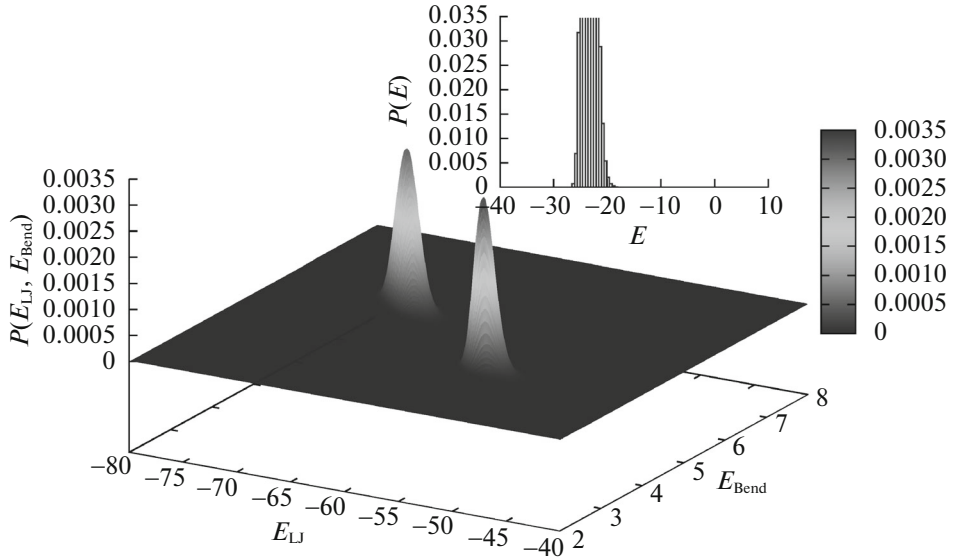

Fig. 3. Energy distribution $P(E_{\rm LJ}, E_{\rm Bend})$ of a 28mer at the transition into the knot phase (D3 $\to$ K5$_1$ for $\kappa = 8$ at $T \approx 0.18$), signaling a clear phase coexistence. The corresponding distribution $P(E)$ of the total energy $E = E_{\rm LJ} + \kappa E_{\rm Bend}$ is shown in the small panel in the back.

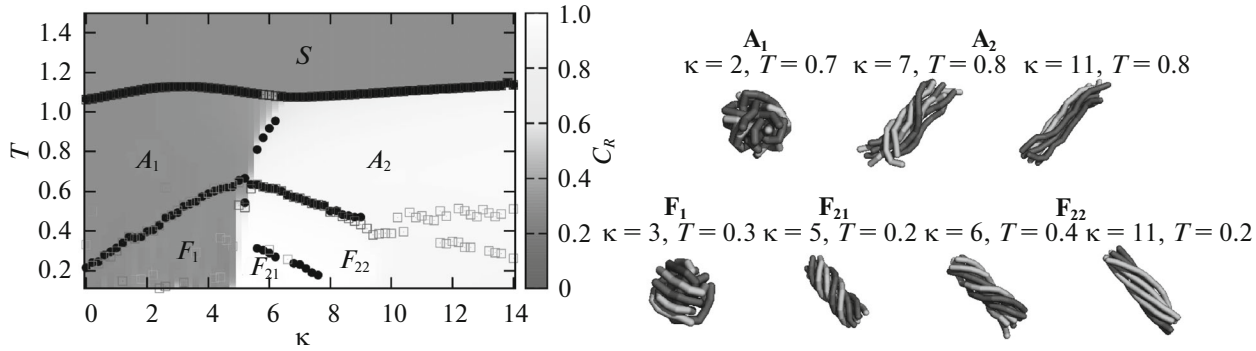

Fig. 4. Temperature—bending stiffness phase diagram of 8 semiflexible 13mers. The background shading encodes the correlation order parameter C_R (1/3 = uncorrelated; 1 = correlated) and the full dots and open squares represent peaks in the heat capacity and the thermal derivative of the phase separation parameter Γ^2, respectively. The right panel shows typical conformations observed in the simulations.

The transition between the phases with knotted and bended chains exhibits quite a peculiar behavior. Its true nature is only revealed when one considers the *two-dimensional* distribution $p(E_{\rm LJ}, E_{\rm Bend})$ of the two partial energies in (5). Fig. 3 shows two clearly separated peaks corresponding to the bended (front) and knotted (back) motifs, implying a first-order like transition. The distribution of the total energy $E = E_{\rm LJ} + \kappa E_{\rm Bend}$ depicted in the inset of Fig. 3, on the other hand, is single-peaked, which would suggest a second-order like transition. The reason is that E is the projection along the diagonal of the two-dimensional distribution for which the two peaks fall on top of each other [21]. This is an example for concealed barriers along an "orthogonal" direction discussed in Sec. 2.3, which prompted us to employ the more elaborate 2DRE and muca+RE simulations instead of just standard muca.

3.2. Aggregation of Semiflexible Polymers

The collapse of polymers or folding of proteins are among the most prominent examples for phase transformations of single macromolecules. In an ensemble of interacting polymers or proteins the interplay with aggregation leads to several other molecular structure formation processes. An important

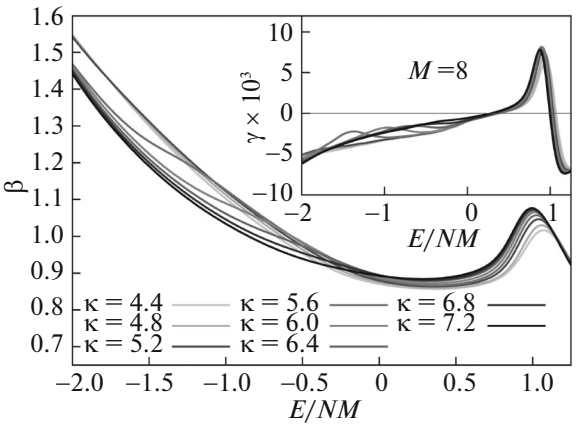

Fig. 5. Microcanonical analysis of the aggregation process. The first (β) and second (γ) derivatives of the microcanonical entropy for $M = 8$ semiflexible 13mers signal an additional transition ($A_1 \to A_2$) of second order ($\gamma < 0$ peaks) for intermediate bending stiffness besides the first-order like aggregation transition ($\gamma > 0$ peaks).

and extensively studied example is the extracellular aggregation of the $A\beta$ peptide, which is associated with Alzheimer's disease.

Extending earlier work mainly for flexible homo- and heteropolymers [16, 27–30], we have recently performed a systematic investigation of the influence of bending rigidity on the aggregation process of homopolymers [31]. The intermolecular interactions of the polymers were assumed to be of the same 12-6 Lennard–Jones type as the intramolecular interaction among the monomers of the same polymer. Instead of stiff bonds here we considered elastic bonds described by the finitely extensible nonlinear elastic (FENE) potential $V_{\mathrm{FENE}}(r) = -\frac{K}{2}R^2 \ln\left(1 - [(r - r_0)/R]^2\right)$ with the "equilibrium" bond length $r_0 = 0.7$, maximal amplitude $R = 0.3$, and spring constant $K = 40$. Matching the solvent-interaction length scale with the bond length, we chose here $\sigma = 2^{-1/6} r_0$. By performing extensive parallelized multicanonical simulations of such an ensemble of M polymers in a cubic box of volume V with periodic boundary conditions, the relevant phase space could be completely covered which, as outlined above, allows one to analyze the system from both the canonical and microcanonical perspective.

To distinguish the fragmented from the aggregated regime, an order parameter $\Gamma^2 = \sum_{i,j} \left(\vec{r}^{\,i}_{\mathrm{cm}} - \vec{r}^{\,j}_{\mathrm{cm}}\right)^2 / (2M^2)$ (with implicit minimal-distance convention for periodic boundary conditions) was introduced that adopts the definition of the squared radius of gyration for a single polymer and basically measures the average spread of the center-of-mass distances $|\vec{r}^{\,i}_{\mathrm{cm}} - \vec{r}^{\,j}_{\mathrm{cm}}|$ of the M chains.

The phase diagram in Fig. 4 for $M = 8$ polymers of length $N = 13$ at monomer density $\rho = MN/V = 10^{-3}$ shows that stiffness plays a crucial role in whether the system forms an amorphous aggregate or a bundle structure. To distinguish these two motifs we introduced the correlation order parameter $C_R = \frac{2}{M(M-1)} \sum_{i<j} (\hat{\vec{R}}_i \cdot \hat{\vec{R}}_j)^2$, where $\hat{\vec{R}}_i$ is the end-to-end unit vector of the i-th polymer.

By this means we could identify a regime of rather flexible polymers forming amorphous aggregates, an intermediate regime, and a regime of rather stiff polymers forming bundle structures. In the intermediate stiffness regime the microcanonical analysis in Fig. 5 reveals that lowering the temperature first drives the system into an uncorrelated aggregate via a first-order-like transition, shortly followed by a second-order-like transition into the correlated aggregate.

The "frozen" (low-temperature) states in Fig. 4 show a twisted bundle structure if the stiffness is large enough. This sort of structure formation has been reported before in the context of material design, however, for specific interactions usually related to proteins. Our study [31] shows that already a sufficiently high bending rigidity can initiate twisted bundle formation (which may be favored or disfavored by additional specific interactions).

4. SUMMARY

Monte Carlo computer simulations in generalized ensembles are a powerful tool for studying structure formation in macromolecular systems. The self-assembly of structural motifs usually proceeds along narrow pathways in a rather complicated, rugged free-energy landscape which would be difficult to explore in a standard canonical framework. We have demonstrated this for two exemplary problems of polymer physics, namely the phase diagram of a semiflexible polymer displaying, among others, stable phases governed by knotted conformations of specific type, and the aggregation process of semiflexible polymers, where twisted bundles are among the most prominent motifs that emerge at low temperatures.

ACKNOWLEDGMENTS

This work was funded by the Deutsche Forschungsgemeinschaft (DFG) through the Collaborative Research Centre SFB/TRR 102 (project B04) and grant no. JA 483/31-1, the Deutsch-Französische Hochschule (DFH-UFA) through the Doctoral College "$\mathbb{L}^4$" under grant no. CDFA-02-07, and by the EU IRSES Network DIONICOS under grant no. 612 707.

REFERENCES

1. W. Janke and W. Paul, "Thermodynamics and structure of macromolecules from flat-histogram Monte Carlo simulations (invited review)," Soft Matter **12**, 642–657 (2016).
2. J. Zierenberg, M. Marenz, and W. Janke, "Dilute semiflexible polymers with attraction: collapse, folding and aggregation (invited review)," Polymers **8**, 333-1–19 (2016).
3. B. A. Berg and T. Neuhaus, "Multicanonical algorithms for first order phase transitions," Phys. Lett. B **267**, 249–253 (1991).
4. B. A. Berg and T. Neuhaus, "Multicanonical ensemble: a new approach to simulate first-order phase transitions," Phys. Rev. Lett. **68**, 9–12 (1992).
5. W. Janke, "Multicanonical simulation of the two-dimensional 7-state Potts model," Int. J. Mod. Phys. C **03**, 1137–1146 (1992).
6. W. Janke, "Multicanonical Monte Carlo simulations," Physica A **254**, 164–178 (1998).
7. K. Hukushima and K. Nemoto, "Exchange Monte Carlo method and application to spin glass simulations," J. Phys. Soc. Jpn. **65**, 1604–1608 (1996).
8. F. Wang and D. P. Landau, "Efficient, multiple-range random walk algorithm to calculate the density of states," Phys. Rev. Lett. **86**, 2050–2053 (2001).
9. F. Wang and D. P. Landau, "Determining the density of states for classical statistical models: a random walk algorithm to produce a flat histogram," Phys. Rev. E **64**, 056101-1–16 (2001).
10. J. Zierenberg, M. Marenz, and W. Janke, "Scaling properties of a parallel implementation of the multicanonical algorithm," Comput. Phys. Commun. **184**, 1155–1160 (2013).
11. J. Zierenberg, M. Marenz, and W. Janke, "Scaling properties of parallelized multicanonical simulations," Phys. Proc. **53**, 55–59 (2014).
12. J. Gross, J. Zierenberg, M. Weigel, and W. Janke, "Massively parallel multicanonical simulations," arXiv:1707.00919 (2017).
13. E. Bittner and W. Janke, "Free-energy barriers in the Sherrington–Kirkpatrick model," Europhys. Lett. **74**, 195–201 (2006).
14. D. H. E. Gross, *Microcanonical Thermodynamics* (World Scientific, Singapore, 2001).
15. W. Janke, "Canonical versus microcanonical analysis of first-order phase transitions," Nucl. Phys. B (Proc. Suppl. A-C) **63**, 631–633 (1998).
16. C. Junghans, M. Bachmann, and W. Janke, "Microcanonical analyses of peptide aggregation processes," Phys. Rev. Lett. **97**, 218103-1–4 (2006).
17. S. Schnabel, D. T. Seaton, D. P. Landau, and M. Bachmann, "Microcanonical entropy inflection points: key to systematic understanding of transitions in finite systems," Phys. Rev. E **84**, 011127-1–4 (2011).
18. P. Schierz, J. Zierenberg, and W. Janke, "First-order phase transitions in the real microcanonical ensemble," Phys. Rev. E **94**, 021301-1–5(R) (2016).
19. J. Zierenberg, P. Schierz, and W. Janke, "Canonical free-energy barrier of particle and polymer cluster formation," Nat. Commun. **8**, 14546-1–7 (2017).
20. M. Marenz and W. Janke, "Effect of bending stiffness on a homopolymer inside a spherical cage," Phys. Proc. **57**, 53–57 (2014).
21. M. Marenz and W. Janke, "Knots as a topological order parameter for semiflexible polymers," Phys. Rev. Lett. **116**, 128301-1–6 (2016).

22. W. Janke and M. Marenz, "Stable knots in the phase diagram of semiflexible polymers: a topological order parameter?," J. Phys.: Conf. Ser. **750**, 012006-1–5 (2016).
23. D. T. Seaton, S. Schnabel, M. Bachmann, and D. P. Landau, "Effects of stiffness on short, semiflexible homopolymer chains," Int. J. Mod. Phys. C **23**, 1240004-1–7 (2012).
24. D. T. Seaton, S. Schnabel, D. P. Landau, and M. Bachmann, "From flexible to stiff: systematic analysis of structural phases for single semiflexible polymers," Phys. Rev. Lett. **110**, 028103-1–5 (2013).
25. P. Virnau, "Detection and visualization of physical knots in macromolecules," Phys. Proc. **6**, 117–125 (2010).
26. L. H. Kauffman, *Knots and Physics,* 2nd ed. (World Scientific, Singapore, 1991).
27. C. Junghans, M. Bachmann, and W. Janke, "Thermodynamics of peptide aggregation processes: an analysis from perspectives of three statistical ensembles," J. Chem. Phys. **128**, 085103-1–9 (2008).
28. C. Junghans, M. Bachmann, and W. Janke, "Statistical mechanics of aggregation and crystallization for semiflexible polymers," Europhys. Lett. **87**, 40002-1–5 (2009).
29. J. Zierenberg, M. Mueller, P. Schierz, M. Marenz, and W. Janke, "Aggregation of theta-polymers in spherical confinement," J. Chem. Phys. **141**, 114908-1–9 (2014).
30. M. Mueller, J. Zierenberg, M. Marenz, P. Schierz, and W. Janke, "Probing the effect of density on the aggregation temperature of semi-flexible polymers in spherical confinement," Phys. Proc. **68**, 95–99 (2015).
31. J. Zierenberg and W. Janke, "From amorphous aggregates to polymer bundles: the role of stiffness on structural phases in polymer aggregation," Europhys. Lett. **109**, 28002-1–6 (2015).